Ultraviolet Photodissociation Spectroscopy of Cold K + •Calix[4]arene Complex in the Gas Phase

ARTICLE *in* THE JOURNAL OF PHYSICAL CHEMISTRY A · JULY 2015

Impact Factor: 2.69 · DOI: 10.1021/acs.jpca.5b05328 · Source: PubMed

6 AUTHORS, INCLUDING:

Yoshiya Inokuchi

Hiroshima University

94 PUBLICATIONS **1,016** CITATIONS

SEE PROFILE

Takayuki Ebata

Hiroshima University

209 PUBLICATIONS **5,222** CITATIONS

SEE PROFILE

THE JOURNAL OF PHYSICAL CHEMISTRY A

Article

pubs.acs.org/JPCA

Ultraviolet Photodissociation Spectroscopy of the Cold K^+·Calix[4]arene Complex in the Gas Phase

Yoshiya Inokuchi,* Kazuki Soga, Kenta Hirai, Motoki Kida, Fumiya Morishima, and Takayuki Ebata

Department of Chemistry, Graduate School of Science, Hiroshima University, Higashi-Hiroshima, Hiroshima 739-8526, Japan

Supporting Information

ABSTRACT: The cooling of ionic species in the gas phase greatly simplifies the UV spectrum, which is of special importance when studying the electronic and geometric structures of large systems, such as biorelated molecules and host−guest complexes. Many efforts have been devoted to achieving ion cooling with a cold, quadrupole Paul ion trap (QIT), but one problem was the insufficient cooling of ions (up to ∼30 K) in the QIT. In this study, we construct a mass spectrometer for the ultraviolet photodissociation (UVPD) spectroscopy of gas-phase cold ions. The instrument consists of an electrospray ion source, a QIT cooled with a He cryostat, and a time-of-flight mass spectrometer. With great care given to the cooling condition, we can achieve ∼10 K for the vibrational temperature of ions in the QIT, which is estimated from UVPD spectra of the benzo-18-crown-6 (B18C6) complex with a potassium ion, K^+·B18C6. Using this setup, we measure a UVPD spectrum of cold calix[4]arene (C4A) complex with potassium ion, K^+·C4A. The spectrum shows a very weak band and a strong one at 36018 and 36156 cm^{-1}, respectively, accompanied by many sharp vibronic bands in the 36000−36600 cm^{-1} region. In the geometry optimization of the K^+·C4A complex, we obtain three stable isomers: one endo and two exo forms. On the basis of the total energy and UV spectral patterns predicted by density functional theory calculations, we attribute the structure of the K^+·C4A complex to the endo isomer (C_2 symmetry), in which the K^+ ion is located inside the cup of C4A. The vibronic bands of K^+·C4A at 36 018 and 36 156 cm^{-1} are assigned to the $S_1(A)-S_0(A)$ and $S_2(B)-S_0(A)$ transitions of the endo isomer, respectively.

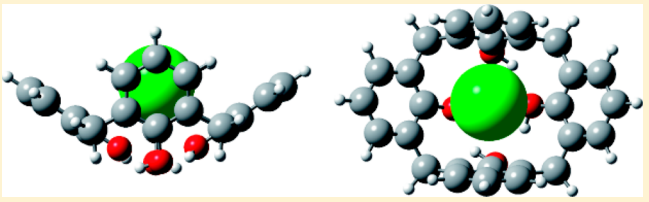

1. INTRODUCTION

Calixarenes (CAs) are macrocycle compounds consisting of phenol units, and they exhibit encapsulation and self-assembly.[1] Their cuplike forms provide cavities to include guest species and show the guest selectivity, which can be controlled by the ring size and introduction of functional groups. Alkali metal ion−CA complexes were extensively studied as simple systems of charged guest−CA complexes. Izatt and co-workers examined cation transport through a liquid membrane system containing CA carriers and discussed the selectivity of alkali metal ions by CAs.[2] In the condensed phase, the conformation of CA complexes with alkali metal ions was determined by X-ray diffraction and NMR spectroscopy.[3] The stoichiometry of CA complexes and the guest selectivity of CAs in solutions were studied by mass spectrometric methods, coupled with electrospray ionization (ESI) and matrix-assisted laser desorption/ionization (MALDI).[4−8] In organic chemistry, Shinkai and co-workers synthesized a number of CA derivatives and succeeded in controlling their conformations, such as cones and partial cones.[9−13] They also demonstrated that the metal ion selectivity of CAs is highly dependent on their conformations. Furthermore, Haino and co-workers synthesized polymeric compounds formed with CAs and guest species such as fullerenes.[14] Laser-based spectroscopy for complexes in the gas phase, coupled with cooling techniques such as free jet expansion and cold ion traps, is also useful for determining the complex structure without the interference from solvent. The cooling of neutral or ionic species in the gas phase greatly simplifies the UV spectrum, which makes it possible to separate features from different stable conformers and examine the electronic and geometric structures individually. Concerning the spectroscopy of CAs in the gas phase, we have investigated the structure of cold inclusion complexes of calix[4]arene (C4A) with neutral guests such as rare gas atoms, water, ammonia, molecular nitrogen, methane, and acetylene under free jet conditions.[15−18] The experimental and theoretical results suggest that all of the inclusion complexes of C4A preferentially form endo complexes (the guests are inside the C4A cup). In addition to the inclusion ability, the electronic structure of C4A is also of great interest. Bare C4A has C_4 symmetry with its four phenol moieties, which interact with each other via a through-space interaction. As a result, C4A exhibits a weak S_1-S_0 transition at 35 357 cm^{-1} and a strong S_2-S_0 transition at 35 521 cm^{-1}.[15] It will be quite interesting to see how the inclusion of ionic species affects the geometric and electronic structure of C4A. For electronic spectroscopy of ionic species, ultraviolet photodissociation (UVPD) spectroscopy is a very powerful technique. Boyarkin, Rizzo, and their co-workers reported pioneering work for the UVPD spectroscopy of cold protonated amino acids with a cold, 22-pole ion

Received: June 4, 2015
Revised: July 10, 2015
Published: July 17, 2015

DOI: 10.1021/acs.jpca.5b05328
J. Phys. Chem. A 2015, 119, 8512−8518

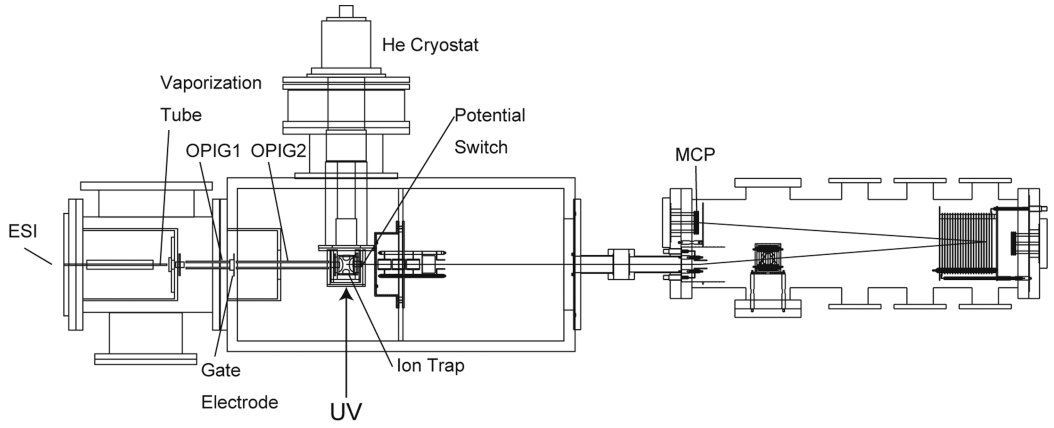

Figure 1. Schematic drawing of a mass spectrometer used in this study.

trap.[19,20] Kim and co-workers extensively studied the UVPD spectroscopy of ion encapsulation complexes of benzo-crown ethers.[21−26] Recently, we have investigated benzo-crown ether complexes with metal ions and their hydrated species, coupled with IR−UV double-resonance spectroscopy, to determine the structure and the number of conformers and to shed light on the origin of the ion selectivity.[27−31]

In the present study, we construct a mass spectrometer for UVPD spectroscopy, equipped with an ESI ion source and a cold, quadrupole Paul ion trap (QIT). First we determine the ion temperature in the QIT by recording the UVPD spectra of the benzo-18-crown-6 (B18C6) complex with the potassium ion, K^+·B18C6. In our previous paper, we measured a UVPD spectrum of cold K^+·B18C6 in a cold, 22-pole ion trap.[28] We estimate the ion temperature of K^+·B18C6 in the QIT by comparing the UVPD spectra using the QIT and the 22-pole ion trap. Then we observe the UVPD spectrum of the C4A complex with the potassium ion, K^+·C4A. We determine the geometric and electronic structure of the K^+·C4A complex from the UVPD spectrum, with the aid of quantum chemical calculations.

2. EXPERIMENTAL AND COMPUTATIONAL METHODS

Figure 1 shows a schematic drawing of a mass spectrometer used in this study. Ion complexes are produced continuously at atmospheric pressure by an ESI source. A stainless steel needle (Hamilton 21033A) is connected to a syringe (Hamilton 1010TLL) through a $^1/_8$ in. Teflon tube, and a solution is carried from the syringe to the needle by a syringe pump (KD Scientific 780-100E) with a flow rate of ∼0.2 mL/h. A high dc voltage (∼3 kV) is applied to the needle for the electrospray. A vaporization tube (a stainless steel tube with an outer diameter of $^1/_{16}$ in. and a length of ∼300 mm) is situated at the entrance of the vacuum chamber. The tube is held by two copper blocks, surrounded by a rubber heater, and heated to ∼100 °C. After passing through the tube and a skimmer with a diameter of 1 mm, ions are introduced into the first octopole ion guide (OPIG). At the exit of the OPIG, a gate electrode is situated to bunch the continuous ion current. This electrode is kept grounded for ∼100 ms, and then a pulsed potential of −30 V with a width of ∼200 μs is applied for the ions to exit the first OPIG. The pulsed ion beam is guided by the second OPIG and introduced into a QIT (Jordan TOF Products C-1251). The QIT is bolted in a copper box, which is connected to the second stage of a He cryostat (Sumitomo Heavy Industries RDK-408D2) and cooled to ∼4 K. The QIT is used in an open configuration; the ring electrode and the end caps are held with four threaded rods and ceramic spacers, and ceramic rings between the ring electrode and the end caps are not used. The copper box is surrounded by a copper shield, which is moderately cooled by the first stage of the He cryostat. A He gas line is attached to the first stage of the cryostat to precool He buffer gas, and then the buffer gas is continuously introduced into the QIT. The ions are stored in the QIT for ∼95 ms and cooled translationally and internally by collision with the cold He buffer gas. Ions other than parent ions of interest are removed from the QIT by an rf potential applied to the entrance end cap, as was done by Kang et al.[32] The parent ions are then irradiated with a UV laser, inducing the dissociation of the ions. After ∼1 μs of UV excitation, resulting fragment ions are accelerated to a homemade time-of-flight mass spectrometer by pulsed potentials applied to the exit end cap and a potential switch located at the exit of the trap and are detected by a multichannel plate (MCP).[33] Output from the MCP is fed into a digital storage oscilloscope (LeCroy Wave Runner 604Zi) or a multichannel scaler/average (Stanford Research Systems SR430). A signal averaged by the oscilloscope or counted by the scaler/averager is transferred to a personal computer through a USB or a GPIB interface. Yields of the fragment ions are normalized by the intensity of the UV laser, and UVPD spectra of the parent ions are obtained by plotting the normalized yields of the fragment ions against the wavenumber of the UV laser. In the experiments on K^+·B18C6 and K^+·C4A, we use a solution containing potassium chloride and B18C6 or C4A (∼100 μM each) dissolved in methanol.

In the UVPD experiments described above, the rf voltages to the OPIGs are generated by rf power supplies, which are constructed on the basis of the rf circuit by Jones and Anderson.[34] The QIT is driven by a power supply for QITs (Jordan TOF Products, D-1203). The pulsed voltage to the exit end cap for ejecting the fragment ions is also supplied by the same power supply. A function generator (Stanford Research Systems DS345) is used to generate the rf voltage to the entrance end cap for removing unnecessary ions from the QIT. The pulsed voltages to the gate electrode and the potential switch are generated by high-voltage pulse generators (DEI PVX-4140). All of the pulsed components are controlled by a digital delay/pulse generator (Berkeley Nucleonics Corporation, model 575). The temperature of the copper box holding the QIT is measured by a silicon diode (Lake Shore Cryotronics, DT-670B-CU) and a cryogenic temperature

DOI: 10.1021/acs.jpca.5b05328
J. Phys. Chem. A 2015, 119, 8512−8518

controller (Lake Shore Cryotronics, model 325). To ensure good thermal contact in the cold components, we use cryogenic high-vacuum grease (M&I Materials Apiezon N) on all of the contact surfaces of the copper components and the ceramic spacers of the QIT.

The tunable UV light is obtained by second-harmonic generation (SHG) of a fundamental output of a pulsed dye laser (Continuum ND6000) pumped by the third harmonic of a Nd:YAG laser (Continuum Surelite II) with a repetition rate of 10 Hz. For the SHG, we use a commercial servo system (Inrad Autotracker II) with a KDP crystal. The UV laser is focused into the QIT loosely by using a quartz lens with a focal length of 3000 mm. A typical output energy of the UV laser used in this study is ∼0.2 mJ/pulse.

We also perform quantum chemical calculations for the K^+·C4A complex and bare C4A. The geometry optimization is performed at the M05-2X/6-31+G(d) level of theory using the Gaussian 09 program package.[35] The transition energy and the oscillator strength are obtained theoretically by time-dependent density functional theory (TD-DFT) calculations at the M05-2X/6-31+G(d) level.

3. RESULTS AND DISCUSSION

First we estimate the ion temperature in our cold QIT by observing the UV spectra of K^+·B18C6. Figure 2 shows the

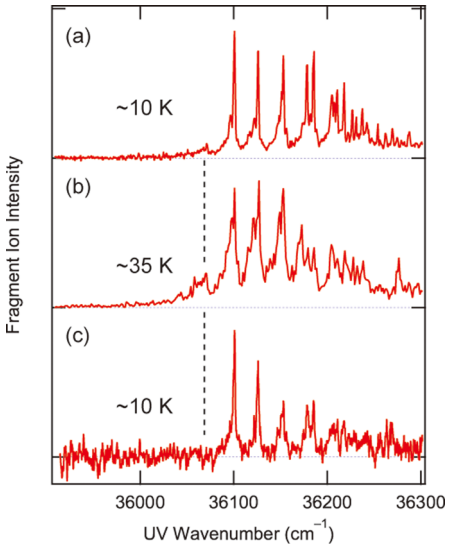

Figure 2. UVPD spectra of the K^+·B18C6 complex measured by using (a) a cold, 22-pole ion trap[28] and (b, c) the cold, quadrupole Paul ion trap in this study.

UVPD spectra of the K^+·B18C6 complex in the 35 900−36 300 cm^{-1} region; these spectra are recorded by detecting the fragment K^+ ion. In our previous study, we recorded the UVPD spectrum of K^+·B18C6 using a cold, 22-pole ion trap (Figure 2a).[28] The origin band appears at 36 101 cm^{-1}, and a weak hot band is seen at 36 071 cm^{-1}. We estimated the ion temperature in Figure 2a to be ∼10 K from the relative intensity and frequency of the hot band.[28] The UVPD spectra in Figure 2b,c were recorded in the present study. When ion cooling is not sufficient (Figure 2b), the relative intensity of the hot band at 36 071 cm^{-1} with respect to the origin band is higher than that in Figure 2a; the vibrational temperature of K^+·B18C6 in Figure 2b is estimated to be ∼35 K, which is a typical value with cold Paul ion traps.[21,36,37] In addition, the width of each vibronic band in Figure 2b is larger than that of the cold spectrum in Figure 2a. Broad features on the lower-frequency side of each band maximum were ascribed to hot bands accompanied by the hot band at 36 071 cm^{-1}.[21] However, by taking great care to avoid the heat flow from electric connections and the He gas line and by optimizing the experimental conditions such as the trapping time and the intensity of the UV laser, we can finally obtain a colder UV spectrum, as shown in Figure 2c. The width of each band becomes sharper than that in Figure 2b, and no noticeable hot band is seen at 36 071 cm^{-1}. From the comparison of the spectra in Figure 2a,c, we estimate the ion temperature in our QIT (Figure 2c) to be ∼10 K. This result indicates that ions can be cooled to ∼10 K even by using Paul ion traps. One can find the difference in the relative intensity of the progression above 36 140 cm^{-1} with respect to the origin band between panels a and c of Figure 2. This is probably due to the saturation effect on the UVPD spectrum in Figure 2a. In the recording of the spectrum in Figure 2a, the UV laser power was ∼1.5 mJ/pulse (though the photon density in the 22-pole ion trap was not measured), which overly enhanced the relative intensity of the weak bands above 36 140 cm^{-1} with respect to the origin band. For the UVPD spectrum in Figure 2c, we decrease the UV power as much as possible to avoid saturation. (The intensity of the fragment K^+ ion in Figure 2c is about ∼20% of that in Figure 2b.) However, since the intensity of the vibronic band at 36 126 cm^{-1} relative to the origin band at 36 101 cm^{-1}, which was used for the evaluation of the vibrational temperature, does not change very much between panels a and c of Figure 2, the previous temperature estimation of the K^+·B18C6 complex in Figure 2a as ∼10 K is still reliable.[28]

Then we observe a UVPD spectrum of the K^+·C4A complex by using our cold QIT. Figure 3 shows the UVPD spectrum of

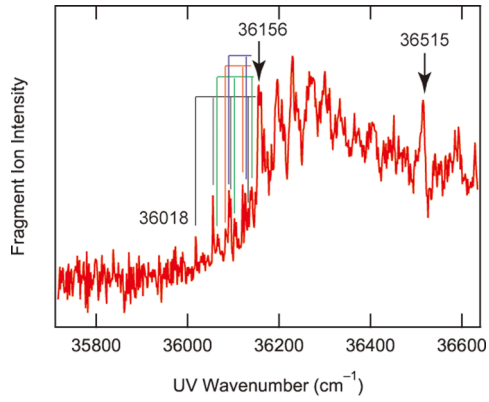

Figure 3. UVPD spectrum of the K^+·C4A complex. Solid lines show low-frequency progressions with an interval of ∼38 cm^{-1}. The spectrum in the 36 000−36 600 cm^{-1} region is obtained by averaging 10 repeated scans. Therefore, the fluctuation of the intensity in the region below 36 000 cm^{-1} is larger than that above it.

the K^+·C4A complex in the 35 700−36 600 cm^{-1} region. The spectrum is measured by monitoring the yield of the fragment K^+ ion. Since the ion intensity of the K^+·C4A complex is much weaker than that of the K^+·B18C6 complex in our experiment, the signal-to-noise ratio of the UVPD spectrum (Figure 3) is not good compared to that of K^+·B18C6 (Figure 2). In spite of the disadvantage of the ion intensity, the cooling of the ions to ∼10 K enables us to observe weak but sharp vibronic bands clearly for K^+·C4A. A very weak but reproducible band is

DOI: 10.1021/acs.jpca.5b05328
J. Phys. Chem. A 2015, 119, 8512−8518

observed at 36 018 cm^{-1} with a bandwidth of ~1.8 cm^{-1} (fwhm). Since no band is observed on the lower-frequency side, the band at 36 018 cm^{-1} can be assigned to the origin band of the S_1-S_0 transition. Jet-cooled C4A shows the origin band of the S_1-S_0 transition at 35 357 cm^{-1}; the attachment of the K^+ ion shifts the electronic transition of C4A to the blue by ~660 cm^{-1}.[15] Such a large blue shift is also observed for the K^+·(dibenzo-18-crown-6) complex.[27] As seen in Figure 3, low-frequency progressions are observed from the origin and other low-frequency bands with an interval of ~38 cm^{-1}. The spectrum is quite congested in the 36 000−36 400 cm^{-1} region, but a strong band clearly appears at 36 156 cm^{-1}, highlighted by an arrow in Figure 3. In addition, another strong band is found at 36 515 cm^{-1}.

On the basis of calculated results of stable isomers and electronic transitions, we attribute the structure of the K^+·C4A complex in our experiment to an endo isomer. Figure 4 displays the stable structure of C4A and K^+·C4A calculated at the M05-2X/6-31+G(d) level of theory. Bare C4A has a C_4 structure with all of the phenol components being identical (C4A-I in Figure 4a).[15] In the case of the K^+·C4A complex, the most-stable structure (KC4A-I in Figure 4b) has its K^+ ion inside the cup (an endo form). The K^+ ion in the second- and the third-most-stable structures (KC4A-II and KC4A-III) is located outside the C4A cup (exo forms), attached to one of the benzene rings and to two of the four oxygen atoms, respectively. The total energy of these isomers relative to that of the most-stable one is quite large (97 and 101 kJ/mol), suggesting that the K^+·C4A complex has a KC4A-I form. This structural assignment of K^+·C4A is confirmed by the results of the TD-DFT calculations. Table 1 shows the calculated transition energies and oscillator strengths for C4A and K^+·C4A. We have demonstrated in our previous study that the relative transition energy of stable isomers obtained by TD-DFT calculations can be used for the structural determination, whereas the absolute values are not consistent with the observed energies.[28] As seen in Table 1, isomers KC4A-I and KC4A-III show the blue shift of the S_1-S_0 transition compared to that of bare C4A (C4A-I). In the case of KC4A-III, the oscillator strengths to the S_1, S_2, and S_3 states have the same order of magnitude. For KC4A-I, in contrast, the oscillator strength to the S_1 state is substantially weaker (almost zero) than that to the S_2 and S_3 states, which reproduces the spectral features of the K^+·C4A complex in Figure 3 much better than KC4A-III. Hence we conclude that the K^+·C4A complex in our experiment has the KC4A-I form. The binding energy between K^+ and C4A for KC4A-I is calculated to be 1.95 eV (15 700 cm^{-1}); this is consistent with the experimental result in which the fragment K^+ ion is formed by the UV excitation of K^+·C4A in the 36 000−36 600 cm^{-1} region.

In KC4A-I (Figure 4b), two of the four benzene rings hold the K^+ ion cooperatively, changing the symmetry from C_4 (bare C4A) to C_2. In Figure 4, the tilting angle of the benzene rings with the principal axis (C_4 or C_2 axis) is shown. The angle of two benzene rings in KC4A-I is substantially lower (13.2°) than that of C4A (34.1°), but the other two benzene rings have a larger angle (55.7°). The distances between the centers of two opposite benzene rings in KC4A-I are 5.77 and 7.63 Å, whereas that of C4A-I is 6.83 Å. We also show the structure of the H_2O·C4A complex (Figure 4e) determined in our previous study.[17] The water molecule is included inside the cup of C4A, but the tilting angles (33.2 and 37.0°) are almost the same as that of bare C4A. Bare C4A forms a hydrogen-bonded ring at the bottom of the cup with four OH groups. The OH stretching vibration of these OH groups is observed at 3158 cm^{-1}, which is substantially lower than that of a phenol dimer or trimer.[15] This indicates that the four OH groups are strongly hydrogen-bonded in bare C4A. The rigid cup structure of C4A is almost retained in inclusion complexes of neutral guests.[15−18] However, the cation−π interaction between the K^+ ion and the benzene rings highly distorts the C4A cavity to fit the cup size to the K^+ ion and maximize the binding energy.

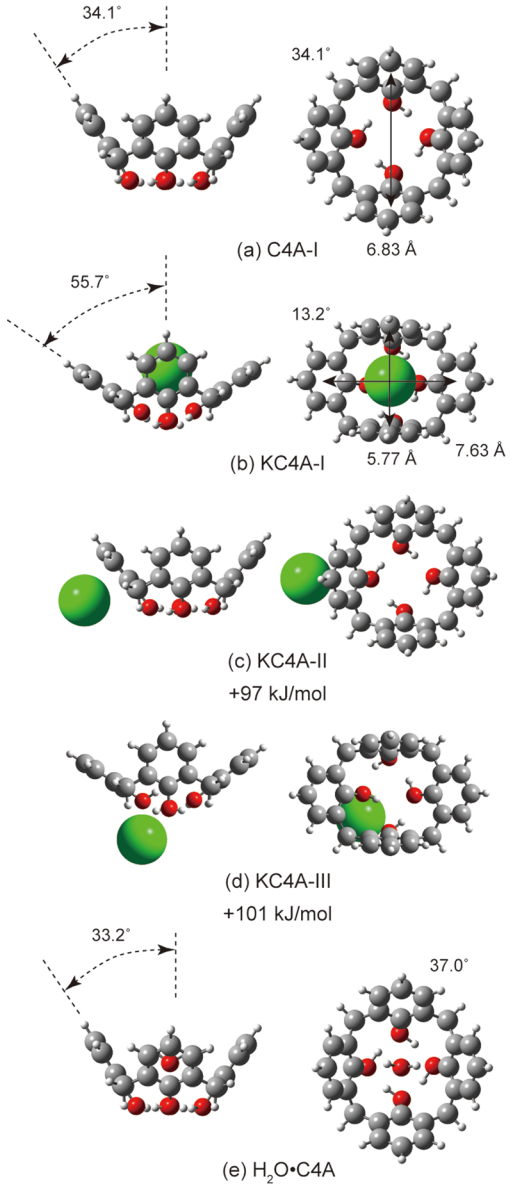

Figure 4. (a−d) Stable structures of C4A and K^+·C4A obtained by the geometry optimization at the M05-2X/6-31+G(d) level of theory. The energy values in panels c and d show the total energy of isomers KC4A-II and KC4A-III relative to that of the most-stable form (KC4A-I). (e) Stable structure of the H_2O·C4A complex determined in our previous study.[17]

Figure 5 shows the comparison of the UVPD spectrum for the K^+·C4A complex with the UV spectrum of jet-cooled C4A; these spectra are plotted as a function of UV wavenumber relative to that of the origin band.[15] One can find similar spectral patterns between C4A and K^+·C4A, namely, a weak S_1-S_0 transition and strong S_2-S_0 and S_3-S_0 transitions. This

DOI: 10.1021/acs.jpca.5b05328
J. Phys. Chem. A 2015, 119, 8512−8518

Table 1. Transition Energy (eV) and Oscillator Strength (in Parentheses) from the Electronic Ground States for C4A and K^+·C4A Calculated at the M05-2X/6-31+G(d) Level of Theory[a]

	C4A-I[b]	KC4A-I[b]	KC4A-II	KC4A-III
S_1	5.09 (0.0001, A)	5.29 (0.0000, A)	4.85 (0.0077)	5.23 (0.0172)
S_2	5.25 (0.1112, E)	5.32 (0.0605, B)	5.02 (0.0902)	5.33 (0.0245)
S_3	5.25 (0.1112, E)	5.33 (0.0744, B)	5.13 (0.0897)	5.34 (0.0402)
S_4	5.38 (0.0000, B)	5.34 (0.0000, A)	5.17 (0.0006)	5.38 (0.0319)

[a]Species of the electronic excited states are in parentheses, only for C4A-I and KC4A-I. [b]C4A-I and KC4A-I have C_4 and C_2 symmetry, respectively.

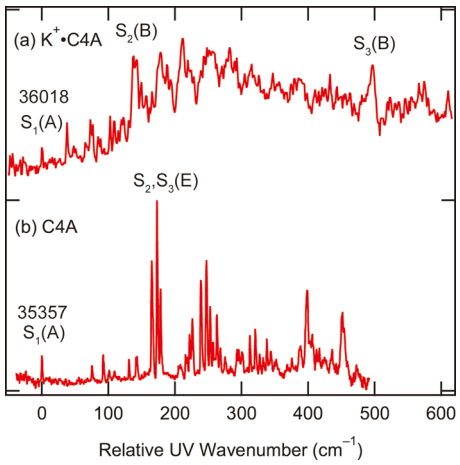

Figure 5. Comparison of the UV spectra of (a) K^+·C4A measured in this study and (b) C4A reported in our previous study (ref 15).

similarity implies that C4A maintains high symmetry upon complex formation with K^+, supporting the assignment of the K^+·C4A structure to KC4A-I (C_2 symmetry). For C4A, the S_1 and S_2 states, which are located ~164 cm^{-1} above the S_1 state, have species A and E with C_4 symmetry.[15] For the K^+·C4A complex, the origin band at 36 018 cm^{-1} and the strong bands at +138 and +497 cm^{-1} can be assigned to the electronic transitions to the S_1 (A), S_2 (B), and S_3 (B) states, on the basis of the result of the TD-DFT calculation for KC4A-I. (In group theory, species E in C_4 symmetry is resolved into two species B in C_2 symmetry.) It should be noted that the S_1−S_0 transition is symmetrically allowed for both of C4A-I and KC4A-I. The very small (almost zero) S_1−S_0 oscillator strength of C4A-I is due to its conformation.[15] The transition dipole moment of each phenol component (to the excited ^1L_b state) is almost parallel to the benzene plane and perpendicular to its C−O bond or perpendicular to the C_4 axis of C4A.[38] Therefore, the transition dipole moment of C4A with species A, which is formed by a linear combination of the transition dipole moments of the phenol parts, is very small, giving a very weak band for the S_1(A)−S_0(A) transition. The UVPD spectrum of K^+·C4A (Figure 5a) and the structure of KC4A-I (Figure 4b) suggest that the above situation of the S_1−S_0 transition for C4A is also likely to be retained for K^+·C4A. Figure 6 displays the molecular orbitals (MOs) of KC4A-I that contribute the most to each electronic transition. Similar to the case of C4A, the transition dipole moment on each phenol component seems to be almost perpendicular to the C_2 axis in K^+·C4A; for instance, in comparing the MOs of the S_2−S_0 transition (Figure 6b) and finding the difference between them, one can recognize that the transition dipole moments of the phenol components are perpendicular to the C_2 axis. Therefore, the resulting transition dipole moment along the C_2 axis is very small, and the S_1(A)−S_0(A) transition is also very weak for K^+·C4A. As seen in Figure

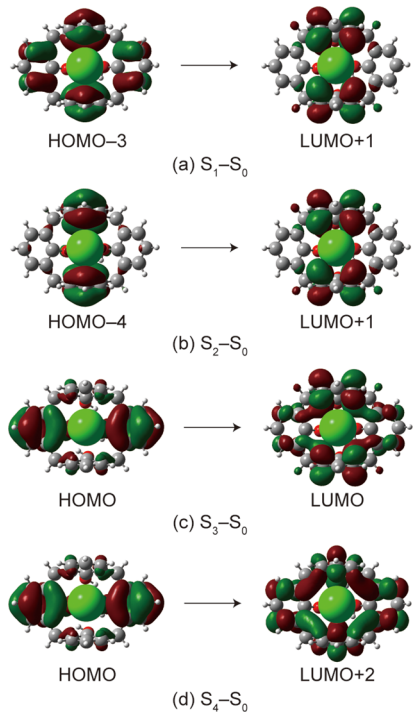

Figure 6. Molecular orbitals of isomer KC4A-I that contribute the most to each electronic transition.

6b, the MOs localized on the pair of benzene rings close to K^+ are involved in the S_2−S_0 transition, having a local excitation nature. In contrast, the S_3−S_0 transition has charge-transfer character from one pair of benzene rings to the other (Figure 6c). Concerning the low-frequency progression with the interval of ~38 cm^{-1} around the origin band, a totally symmetric intermolecular vibration may be involved in it. One candidate for the normal mode of KC4A-I is shown in Figure 1S of the Supporting Information. This is the lowest-frequency vibration (47 cm^{-1}) of KC4A-I in the S_0 state and can be expressed as a large-amplitude deformation motion of the C4A cup.

4. SUMMARY

We have constructed a mass spectrometer equipped with an ESI source and a cold, quadrupole Paul ion trap (QIT). To determine the ion temperature in our QIT, we have recorded the UVPD spectra of the K^+·B18C6 complex and estimated the ion temperature to be ~10 K. We then have observed the UVPD spectrum of the K^+·C4A complex. The spectrum shows a very weak band at 36 018 cm^{-1} and a strong one at 36 156 cm^{-1}, with low-frequency (~38 cm^{-1}) progressions. In the geometry optimization of the K^+·C4A complex, we found three stable isomers. On the basis of the total energy and the results of the TD-DFT calculations, we attribute the structure of the

DOI: 10.1021/acs.jpca.5b05328
J. Phys. Chem. A 2015, 119, 8512−8518

K^+·C4A complex to the endo isomer (KC4A-I), in which the K^+ ion is located inside the cup. Isomer KC4A-I has C_2 symmetry, whereas bare C4A takes a C_4 structure. The symmetry reduction from C_4 to C_2 induced by the attachment of the K^+ ion will provide a different infrared spectrum than that of bare C4A.[15] Izatt and co-workers suggested that C4A derivatives show the greatest selectivity for Cs^+ among alkali metal ions.[2] Klinowski and co-workers concluded in their solid-state NMR studies that each C4A-based molecule holds a Cs^+ ion inside the cup but that Li^+ and Na^+ ions are bonded to the phenolic oxygens.[3] The application of UVPD spectroscopy to other alkali metal ion−CA complexes and the recording of their IR-UV spectra will be of great interest in our future work.

■ ASSOCIATED CONTENT

Supporting Information

A vector drawing of the lowest-frequency vibration of KC4A-I and a full list of authors of ref 35. The Supporting Information is available free of charge on the ACS Publications website at DOI: 10.1021/acs.jpca.5b05328.

■ AUTHOR INFORMATION

Corresponding Author

*E-mail: y-inokuchi@hiroshima-u.ac.jp.

Notes

The authors declare no competing financial interest.

■ ACKNOWLEDGMENTS

This work was partially supported by the Japan Society for the Promotion of Science (JSPS) through the program "Strategic Young Researcher Overseas Visits Program for Accelerating Brain Circulation". Y.I. is grateful to Professor Thomas R. Rizzo and Dr. Oleg V. Boyarkin at École Polytechnique Fédérale de Lausanne and Professor Shun-ichi Ishiuchi at Tokyo Institute of Technology for their valuable comments on ion cooling in ion traps.

■ REFERENCES

(1) Gutsche, C. D. *Calixarene Revised*; Royal Society of Chemistry: Cambridge, U.K., 1998.

(2) Izatt, S. R.; Hawkins, R. T.; Christensen, J. J.; Izatt, R. M. Cation Transport from Multiple Alkali Cation Mixtures Using a Liquid Membrane System Containing a Series of Calixarene Carriers. *J. Am. Chem. Soc.* **1985**, *107*, 63−66.

(3) Benevelli, F.; Kolodziejski, W.; Wozniak, K.; Klinowski, J. Solid-State NMR Studies of Alkali Metal Ion Complexes of P-Tertbutyl-Calixarenes. *Chem. Phys. Lett.* **1999**, *308*, 65−70.

(4) Schalley, C. A.; Castellano, R. K.; Brody, M. S.; Rudkevich, D. M.; Siuzdak, G.; Rebek, J. Investigating Molecular Recognition by Mass Spectrometry: Characterization of Calixarene-Based Self-Assembling Capsule Hosts with Charged Guests. *J. Am. Chem. Soc.* **1999**, *121*, 4568−4579.

(5) Vincenti, M.; Irico, A. Gas-Phase Interactions of Calixarene- and Resorcinarene-Cavitands with Molecular Guests Studied by Mass Spectrometry. *Int. J. Mass Spectrom.* **2002**, *214*, 23−36.

(6) Weimann, D. P.; Schalley, C. A. Host-Guest Chemistry of Self-Assembling Supramolecular Capsules in the Gas Phase. *Supramol. Chem.* **2008**, *20*, 117−128.

(7) Wong, P. S. H.; Yu, X.; Dearden, D. V. Complexes of P-Tert-Butylcalix[4]arene with Mono- and Dipositive Cations in the Gas Phase. *Inorg. Chim. Acta* **1996**, *246*, 259−265.

(8) Zadmard, R.; Kraft, A.; Schrader, T.; Linne, U. Relative Binding Affinities of Molecular Capsules Investigated by ESI-Mass Spectrometry. *Chem. - Eur. J.* **2004**, *10*, 4233−4239.

(9) Ikeda, A.; Shinkai, S. On the Origin of High Ionophoricity of 1,3-Alternate Calix[4]arenes - Pi-Donor Participation in Complexation of Cations and Evidence for Metal-Tunneling through the Calix[4]arene Cavity. *J. Am. Chem. Soc.* **1994**, *116*, 3102−3110.

(10) Ikeda, A.; Shinkai, S. Novel Cavity Design Using Calix[*n*]arene Skeletons: Toward Molecular Recognition and Metal Binding. *Chem. Rev.* **1997**, *97*, 1713−1734.

(11) Iwamoto, K.; Araki, K.; Shinkai, S. Conformations and Structures of Tetra-O-Alkyl-Para-Tert-Butylcalix[4]arenes - How Is the Conformation of Calix[4]Arenes Immobilized. *J. Org. Chem.* **1991**, *56*, 4955−4962.

(12) Iwamoto, K.; Shinkai, S. Syntheses and Ion Selectivity of All Conformational Isomers of Tetrakis((Ethoxycarbonyl)Methoxy)-Calix[4]arene. *J. Org. Chem.* **1992**, *57*, 7066−7073.

(13) Shinkai, S. Calixarenes - the 3rd-Generation of Supramolecules. *Tetrahedron* **1993**, *49*, 8933−8968.

(14) Haino, T.; Hirai, E.; Fujiwara, Y.; Kashihara, K. Supramolecular Cross-Linking of [60]fullerene-Tagged Polyphenyl-Acetylene by the Host-Guest Interaction of Calix[5]arene and [60]fullerene. *Angew. Chem., Int. Ed.* **2010**, *49*, 7899−7903.

(15) Ebata, T.; Hodono, Y.; Ito, T.; Inokuchi, Y. Electronic Spectra of Jet-Cooled Calix[4]arene and Its Van Der Waals Clusters: Encapsulation of a Neutral Atom in a Molecular Bowl. *J. Chem. Phys.* **2007**, *126*, 141101.

(16) Ebata, T.; Hontama, N.; Inokuchi, Y.; Haino, T.; Apra, E.; Xantheas, S. S. Encapsulation of Ar_n Complexes by Calix[4]arene: Endo- Vs. Exo-Complexes. *Phys. Chem. Chem. Phys.* **2010**, *12*, 4569−4579.

(17) Hontama, N.; Inokuchi, Y.; Ebata, T.; Dedonder-Lardeux, C.; Jouvet, C.; Xantheas, S. S. Structure of the Calix[4]arene-(H_2O) Cluster: The World's Smallest Cup of Water. *J. Phys. Chem. A* **2010**, *114*, 2967−2972.

(18) Kaneko, S.; Inokuchi, Y.; Ebata, T.; Apra, E.; Xantheas, S. S. Laser Spectroscopic and Theoretical Studies of Encapsulation Complexes of Calix[4]arene. *J. Phys. Chem. A* **2011**, *115*, 10846−10853.

(19) Boyarkin, O. V.; Mercier, S. R.; Kamariotis, A.; Rizzo, T. R. Electronic Spectroscopy of Cold, Protonated Tryptophan and Tyrosine. *J. Am. Chem. Soc.* **2006**, *128*, 2816−2817.

(20) Svendsen, A.; Lorenz, U. J.; Boyarkin, O. V.; Rizzo, T. R. A New Tandem Mass Spectrometer for Photofragment Spectroscopy of Cold, Gas-Phase Molecular Ions. *Rev. Sci. Instrum.* **2010**, *81*, 073107.

(21) Choi, C. M.; Baek, J. Y.; Park, K. S.; Heo, J.; Kim, N. J. Conformation-Specific Ultraviolet Spectroscopy of Benzo-18-Crown-6 Complexes with a Potassium Cation. *Chem. Phys. Lett.* **2014**, *593*, 150−153.

(22) Choi, C. M.; Choi, D. H.; Heo, J.; Kim, N. J.; Kim, S. K. Ultraviolet−Ultraviolet Hole Burning Spectroscopy in a Quadrupole Ion Trap: Dibenzo[18]crown-6 Complexes with Alkali Metal Cations. *Angew. Chem., Int. Ed.* **2012**, *51*, 7297−7300.

(23) Choi, C. M.; Heo, J.; Choi, M. C.; Kim, N. J. Ejection Process of Photofragment Ions from a Quadrupole Ion Trap. *Int. J. Mass Spectrom.* **2013**, *337*, 12−17.

(24) Choi, C. M.; Kim, H. J.; Lee, J. H.; Shin, W. J.; Yoon, T. O.; Kim, N. J.; Heo, J. Ultraviolet Photodepletion Spectroscopy of Dibenzo-18-Crown-6-Ether Complexes with Alkali Metal Cations. *J. Phys. Chem. A* **2009**, *113*, 8343−8350.

(25) Choi, C. M.; Lee, J. H.; Choi, Y. H.; Kim, H. J.; Kim, N. J.; Heo, J. Ultraviolet Photodepletion Spectroscopy of Dibenzo-18-Crown-6-Ether Complexes with Alkaline Earth Metal Divalent Cations. *J. Phys. Chem. A* **2010**, *114*, 11167−11174.

(26) Kim, H. J.; Shin, W. J.; Choi, C. M.; Lee, J. H.; Kim, N. J. Electronic Photodepletion Spectroscopy of Dibenzo-18-Crown-6 with a Potassium Ion. *Bull. Korean Chem. Soc.* **2008**, *29*, 1973−1976.

(27) Inokuchi, Y.; Boyarkin, O. V.; Kusaka, R.; Haino, T.; Ebata, T.; Rizzo, T. R. UV and IR Spectroscopic Studies of Cold Alkali Metal Ion-Crown Ether Complexes in the Gas Phase. *J. Am. Chem. Soc.* **2011**, *133*, 12256−12263.

DOI: 10.1021/acs.jpca.5b05328
J. Phys. Chem. A 2015, 119, 8512−8518

(28) Inokuchi, Y.; Boyarkin, O. V.; Kusaka, R.; Haino, T.; Ebata, T.; Rizzo, T. R. Ion Selectivity of Crown Ethers Investigated by UV and IR Spectroscopy in a Cold Ion Trap. *J. Phys. Chem. A* **2012**, *116*, 4057−4068.
(29) Inokuchi, Y.; Kusaka, R.; Ebata, T.; Boyarkin, O. V.; Rizzo, T. R. Laser Spectroscopic Study of Cold Host-Guest Complexes of Crown Ethers in the Gas Phase. *ChemPhysChem* **2013**, *14*, 649−660.
(30) Inokuchi, Y.; Ebata, T.; Rizzo, T. R.; Boyarkin, O. V. Microhydration Effects on the Encapsulation of Potassium Ion by Dibenzo-18-Crown-6. *J. Am. Chem. Soc.* **2014**, *136*, 1815−1824.
(31) Inokuchi, Y.; Ebata, T.; Rizzo, T. R. Solvent Effects on the Encapsulation of Divalent Ions by Benzo-18-Crown-6 and Benzo-15-Crown-5. *J. Phys. Chem. A* **2015**, *119*, 8097.
(32) Kang, H.; Féraud, G.; Dedonder-Lardeux, C.; Jouvet, C. New Method for Double-Resonance Spectroscopy in a Cold Quadrupole Ion Trap and Its Application to UV−UV Hole-Burning Spectroscopy of Protonated Adenine Dimer. *J. Phys. Chem. Lett.* **2014**, *5*, 2760−2764.
(33) Kobayashi, Y.; Inokuchi, Y.; Ebata, T. Ion Core Structure in $(CS_2)_n^+$ and $(CS_2)_n^-$ (n = 3−10) Studied by Infrared Photodissociation Spectroscopy. *J. Chem. Phys.* **2008**, *128*, 164319.
(34) Jones, R. M.; Anderson, S. L. Simplified Radio-Frequency Generator for Driving Ion Guides, Traps, and Other Capacitive Loads. *Rev. Sci. Instrum.* **2000**, *71*, 4335−4337.
(35) Frisch, M. J.; Trucks, G. W.; Schlegel, H. B.; Scuseria, G. E.; Robb, M. A.; Cheeseman, J. R.; Scalmani, G.; Barone, V.; Mennucci, B.; Petersson, G. A. et al. *Gaussian 09, Revision A.1*; Gaussian, Inc.: Wallingford, CT, 2009.
(36) Dedonder, C.; Féraud, G.; Jouvet, C. Identification of Daughter Ions through Their Electronic Spectroscopy at Low Temperature. *J. Chem. Phys.* **2014**, *141*, 131101.
(37) Choi, C. M.; Choi, D. H.; Kim, N. J.; Heo, J. Effective Temperature of Protonated Tyrosine Ions in a Cold Quadrupole Ion Trap. *Int. J. Mass Spectrom.* **2012**, *314*, 18−21.
(38) Granucci, G.; Hynes, J. T.; Millié, P.; Tran-Thi, T.-H. A Theoretical Investigation of Excited-State Acidity of Phenol and Cyanophenols. *J. Am. Chem. Soc.* **2000**, *122*, 12243−12253.

DOI: 10.1021/acs.jpca.5b05328
J. Phys. Chem. A 2015, 119, 8512−8518